Egypt.J.Chem. **Vol. 62**, No. 12. pp. 2277- 2288 (2019)

Egyptian Journal of Chemistry
http://ejchem.journals.ekb.eg/

Carbon Xerogel/Carbon Nanotubes Nanohybrid Doped with Ti for Removal of Methylene Blue Dye

Nady A. Fathy*, Sahar M. El-Khouly, Reham M.M. Aboelenin
Physical Chemistry Department, National Research Centre, 33 El Buhouth street, Dokki, Cairo, P.O. 12622, Egypt.

A FACILE technology for decorating carbon xerogel (CX) with carbon nanotubes (CNTs) to prepare carbonaceous nanohybrid (CX-CNTs) was simultaneously implemented during carbonization of resorcinol-formaldehyde xerogel at 1123K meanwhile camphor as carbon nanotubes source is heated at 523K. Then the prepared CX-CNTs hybrid is doped with tetrabutyl orthotitanate as a titanium (Ti) precursor giving CX-CNTs-Ti nanohybrid used as an efficient photocatalyst. The morphology and textural properties of the samples were investigated using field-emission scanning electron microscope (FE-SEM), High resolution transmission electron microscopy (TEM) and N_2 adsorption-desorption isotherm at 77K. The adsorption and photocatalytic properties of these samples toward methylene blue dye (MB) were performed. FE-SEM and TEM approved the formation of CNTs over the surface of CX and the developed nanohybrids have mesoporous structures. The adsorption efficiency of CX-CNTs and CX-CNTs-Ti samples was found to be 70 and 86.8% along 180 min, respectively. Under visible irradiation, the removal efficiency of CX-CNTs and CX-CNTs-Ti is enhanced to 90 and 99% at 60 min, respectively. Thus, CX-CNTs-Ti nanohybrid exhibited superior adsorptivity and photoactivity for removing MB dye as a result of the presence of Ti particles over CX-CNTs matrix. Doping CX-CNTs with Ti particles led to a decrease in the specific surface area and to enhance in both the total pore volume and amount of wider pores. Therefore, the reported CX-CNTs-Ti nanohybrid exhibits as an effective adsorbent and photocatalyst toward the removal of the MB dye from their aqueous solutions.

Keywords: Carbon xerogel, Carbon nanotubes, Nanohybrid, Titanium, Adsorption, Photocatalysis

Introduction

Since the synthesis of carbon gels by Pekala [1], carbon xerogel (CX) has been attracted considerable interests due to their controllable and tunable porosity, surface chemical properties and the possibility of modified the shape of CX in suitable forms, e.g. powder, monoliths, thin films and pellets on a large-scale with low cost production as compared to carbon aerogels and cryogels [2-6]. CX can be synthesized from the carbonization of organic xerogels that are obtained by a sol-gel method. During this method, a polycondensation reaction of certain organic monomers such as resorcinol and formaldehyde in the presence of basic or acidic inorganics such as Na_2CO_3 or HCl as catalysts, takes place, followed by evaporative drying and pyrolysis in an inert atmosphere [5, 6].

Carbon nanotubes (CNTs) which discovered by Iijima [7] have exceptional properties of tubular structure such as aspect surface-to-volume ratio, mechanical strength, electrical and thermal conductivity, which undertake them in numerous applications such as manufacture of membranes, ceramics, electronic devices, fuel cells, and thermal insulators [8, 9]. As well, they

*Corresponding author: Tel.: +20 2 33371433, Fax: +20 2 33370597;
E-mail: fathyna.77@hotmail.com ORCID*: 0000-0002-6522-1053
Received 16/5/2019; Accepted 29/5/2019
DOI: 10.21608/ejchem.2019.12870.1803

can be used as additives, catalyst supports and adsorbents for carrying out different processes including energy storage, catalysis and water/air purification [10-12]. Three known methods are employed for synthesis of CNTs which are arc discharge, laser ablation and the chemical vapor deposition (CVD) [8]. However, CVD process is the most favorable method for producing high yields of CNTs on industrial scale-up.

Of late, carbonaceous nanohybrids consisting of carbon gels and carbon nanotubes having a promoted synergistic effect leading to form unique surface, thermal, mechanical and electrical properties which make them promising in separation, catalysis and energy storage applications. For this purpose, recent technologies have been carried out to incorporate commercial CNTs into the network of organic aerogels during sol-gel polymerization of resorcinol and formaldehyde (RF) in an aqueous solution using surfactants or organic solvents [13-17]. Through another way, Fu et al. [18] synthesized CNTs on cobalt-doped carbon aerogels either by carbon monoxide decomposition at 1123K under flowing of argon gas. Baumann and co-workers [19] prepared carbon aerogels /CNTs nanohybrids through the CVD method. Fathy et al. [20] synthesized carbon nanotube/carbon xerogel hybrid (CNT/CX) during CVD of camphor over carbonized RF xerogel loaded with nickel catalyst at 1123K. It has been found that CNT/CX nanohybrid possesses a superior capacitance as compared to the individual component of CX or CNTs.

The current study aims at preparing CX-CNTs nanohybrids doped with titanium particles (Ti) as photocatalyst source for determining their adsorption and photodegradation performances toward the removal of methylene blue (MB) dye from aqueous solutions. The CX-CNTs sample was prepared according to the procedure reported elsewhere [20]. Titanium particles were doped on CX-CNTs using tetrabutylorthotitanate (TBOT) as titanium precursor at mass ratio of 4:1 (CX-CNTs/TBOT) in order to hybridize the photoactivity of Ti with the adsorption of CX-CNTs to remove MB dye from aqueous solutions.

Materials and Methods

Materials

Resorcinol ($C_6H_4(OH)_2$, 99 %) was obtained from Panreac. Formaldehyde solution (HCHO, 36-38%), methanol (CH_3OH, 99%) and tetrabutyl orthotitanate (TBOT, $Ti(OCH_2CH_2CH_2CH_3)_4$, 97%) were purchased from Sigma-Aldrich. Acetic acid (CH_3COOH, 96 %) was obtained from El-Nasr Pharmaceuticals Co., Egypt. Ferric nitrate ($Fe(NO_3)_3.9H_2O$) was supplied from SDFCL, India and nickel nitrate ($Ni(NO_3)_2{\cdot}6H_2O$) was obtained from BDH, Germany.

Preparation of Resorcinol-formaldehyde organic xerogel

The RF xerogel was prepared by polycondensation of resorcinol (R) with formaldehyde (F) in molar ratio of 1:2. Briefly, 56.6 g of R was added to 113 ml of distilled water in a glass flask. After complete dissolution, 82 ml of F solution stabilized with 15 wt.% methanol was introduced into the flask. After that, a calculated amount of acetic acid as acid catalyst was added with molar ratio R/C=500, under stirring at 353 K. The initial pH of the sol was adjusted to 6 by adding 0.1 M of NaOH solution. The gelation step was allowed to proceed at 353 K during 48h. After this period, the gel was dark red and the consistency of the material allowed the sample to be shaped as desired (ground to small particles ca. 0.1 mm). The RF hydrogel was further dried within temperature scheme in an air-oven as follows: 373 K for 90 min, 393K for 120 min and then at 423 K for 180 min to get RF xerogel and then kept in closed glass tubes.

Preparation of carbon xerogels/carbon nanotubes nanohybrids

Firstly, RF xerogel sample was impregnated with about 10 wt.% of ferric nitrate and nickel nitrate which dissolved at least amount of H_2O, respectively. The impregnated RF xerogel was dried at in an oven at 353K overnight.

Chemical vapor deposition (CVD) unit comprising two separated chambers, fixed on a desk, was employed for the synthesis of carbon xerogel/carbon nanotubes nanohybrid. A stainless steel tube (diameter=3.2 cm and length=80 cm) was placed in a horizontal position throughout two electric furnaces. Commercial camphor was used as hydrocarbon source since it is inexpensive, nontoxic and commercially available. About 3 g of camphor was put into an alumina boat and kept inside the first furnace in which cracking of camphor sample took place under flowing nitrogen gas. In the 2nd unit, 0.6 g of RF xerogel impregnated with Fe and Ni nitrates in the 2nd chamber was firstly heated upon 923K under flowing N_2 gas for 60 min. Consequently,

camphor was heated at 523K to get the mixture in a gas phase, while, the temperature of 2nd furnace was set at 1123K for growing CNTs on the surface of pyrolyzed RF xerogel. The vapors liberated from camphor were moved to the 2nd furnace with high temperature by a N_2 gas flow. After 30 min, the two furnace units were switched off and the resulting product was labeled as CX-CNTs.

Preparation of Ti loaded on CX-CNTs nanohybrid

Before loading titanium particles on the surface of CX-CNTs to prepare CX-CNTs-Ti nanohybrid, the parent CX-CNTs was primarily oxidized with concentrated acids (HNO_3/ H_2SO_4= 3/1 v/v). A powder of CX-CNTs sample was mixed with a solution of concentrated acids in a round bottle and heated at 333 K under stirring for 4h. To remove the acidic solution, the dispersed nanohybrid in the acidic solution was centrifuged for 30 min (1000 rpm). Then, it was filtrated, washed with distilled water for several times and dried at 333K overnight. After that, TBOT solution was used as Ti precursor at mass ratio of 4:1 (CX-CNTs to TBOT).

Firstly the CX-CNTs was dispersed in 30 mL of H_2O using an ultrasonic (30 min). TBOT was dissolved in 30 mL HNO_3 (1M) solution and stirred for 120 min to give transparent TiO_2 sol, then 0.1M NaOH was added to adjust pH at 3 forming a turbid TiO_2 colloid. TiO_2 colloid was diluted by adding 200 mL H_2O and then added to the dispersed nanohybrid in a round bottle and heated to 333K under stirring for 3h. Then, a 0.5mL of hydrazine hydrated was added to the mixture in order to form Ti (IV) particles coated the nanohybrid. After cooling the reaction, the mixture was centrifuged at 1000 rpm for 60 min to separate the nanohybrid and then washed thoroughly with distilled water for several times and then dried at 363 K overnight to get the final product "CX-CNTs-Ti".

Characterization of nanohybrids

Before and after formation of CNTs, the surface structure and chemical compositions of the prepared samples were described by field-emission scanning electron microscope (SEM) combined with energy-dispersive spectroscopy and electron backscatter diffraction (FE-SEM, FEI Quanta FEG-250, EDS). High resolution transmission electron microscopy (HR-TEM, JEM-1230, Japan) was used to determine the morphologies of the resulting nanohybrids.

The principal porous properties of the obtained nanohybrids were evaluated by nitrogen adsorption analysis at 77 K during an automated adsorption gas apparatus ((BEL-Sorp, Microtrac Bel Crop, Japan). Prior to nitrogen adsorption analysis, the samples were degassed at 473K under a vacuum for several hours, and the isotherms were measured in the relative pressure (P/P_0) range of 0.01- 0.99. Major textural parameters such as the specific surface area, total pore volume and pore width were estimated from N_2 adsorption-desorption isotherms by applying the Brunauer-Emmet-Teller (BET) method [21]. The BET analysis was employed for relative pressure between 0.01 and 0.3 to deduce the total surface area (S_{BET}, m^2/g) and the total pore volume (V_P, cm^3/g) was calculated from the amount of vapor adsorbed at $P/P_0 = 0.975$. The pore width (W_p, Å) was calculated from $(4V_T/S_{BET}) \times 10^4$. In addition Harkins-Jura equation (t-plot) [22] was used to determine the specific internal surface area ($S_{micro\text{-t-plot}}$, m^2/g) and the specific micropore volume ($V_{micro\text{-}\mathbf{t\text{-}plot}}$, cm^3/g) [23]. The mesopore volume was deduced from $(V_{meso\text{-t-plot}}) = V_p - V_{micro}$, assuming that macropores are negligible.

Adsorption and photodegradation of MB dye

Methylene blue is a basic dye with heterocyclic aromatic chemical moiety. The molecular formula is $C_{16}H_{18}ClN_3S$ with absorption maxima at 668 nm. The dye stock solution 100 mg/L was prepared by dissolving 0.1 g dye in 1L distilled water. The experimental solutions were obtained by diluting the dye stock solution to the desired initial concentrations (10, 20 and 50 mg/L).

To assess the adsorption performance of the prepared nanohybrids, the adsorption kinetic experiments were carried out using 25 mL of MB dye (10mg/L) and 10 mg of each nanohybrid at different time intervals from 5 to 180 min at room temperature and at pH 6.

Photodegradation experiments were performed using 10 and 20 mg of CX-CNTs-Ti nanohybrid with 25 mL of MB dye solution (10 and 25 mg/L) in order to study the effects of catalyst loading and dye concentration at constant pH 6. A 150 W fluorescent lamp household light was used as a visible light source. It irradiates outside at 10 cm a distant from the solution surface. Prior to visible irradiation, the mixture was magnetically stirred in the darkness for 30 min in order to reach the steady state of adsorption equilibrium on the surface of nanohybrid. A 0.25 mL of the dye solution was taken at certain interval time, which diluted to 5 mL by distilled water and then centrifuged at 1000

rpm for 10 min to get a clear residual dye solution. The residual MB concentration was estimated by measuring their absorbance at 664 nm using a by UV-Vis spectrophotometer (Shimadzu-PC2401). The removal efficiency (% R) of MB dye was calculated using the following equation:

$$\% R = \frac{(C_0 - C_e)\ 100}{C_0} \quad (1)$$

Where C_0 and C_e are the initial and equilibrium liquid-phase concentrations of dye in aqueous solution (mg/L), respectively.

Kinetic models

The kinetic tests were carried out following the same procedure used for adsorption and photocatalytic degradation of MB dye under dark and visible light irradiation operations. Aliquots samples were taken at different intervals of time and the concentrations of MB were measured at the same intervals. The amount of MB (q_t, mg/g) removed by the obtained nanohybrid at time t (min), was calculated by means of the expression below:

$$q_t = \frac{(C_0 - C_t)\,V}{m} \quad (2)$$

Where C_0 and C_t are the liquid-phase concentrations (mg/L) at an initial and pre-determined time t (min) , respectively, V the volume of solution (L) and m is the dry weight of the added photocatalyst (g). In addition, the kinetic data for MB dye adsorption and MB dye degradation were then fitted into the pseudo–first order, pseudo–second order and intraparticle diffusion models.

The rate constant of adsorption was determined from the pseudo–first order equation proposed by Lagergren [24]:

$$\log (q_e - q_t) = \log q_{el} - \frac{k_1 t}{2.303} \quad (3)$$

Where qe and qt are the amounts of MB degraded at equilibrium (mg/g) and at time t (min), respectively and k1 is the degradation rate constant (min –1).

The pseudo–second order equation based on the equilibrium adsorption is expressed as [25]:

$$\frac{t}{q_t} = \frac{1}{k_2 q_{e2}^{\ 2}} + \frac{t}{q_{e2}} \quad (4)$$

Where k_2 (g/mg. min) is the rate constant of second-order degradation.

The intraparticle diffusion model was further used to identify the importance of diffusion during adsorption process of MB onto the nanohybrids under dark. The intraparticle diffusion equation most-widely applied for adsorption system was proposed by Weber and Morris as following [26]:

$$q_t = K_{id}\, t^{1/2} + C_i \quad (5)$$

Where k_{id} , $t^{1/2}$ and C_i are the intraparticle diffusion rate constant (mg/ g.min$^{1/2}$), square root of the time (min)$^{1/2}$, and intercept at stage *i*, respectively. The value of C_i is related to the thickness of boundary layer. The extrapolation of the linear straight lines to the time axis gives intercepts C_i. If C_i is equal to zero, the only controlling step is intraparticle diffusion. However, if $C_i \neq 0$, indicates that the adsorption process is rather complex and involves more than one diffusive resistance.

Results and Discussion

Surface and Textural features of nanohybrids

Fig.1. shows the FE-SEM photographs of carbon xerogels before and after decoration with carbon nanotubes as prepared by CVD of camphor powder as carbon source over carbon xerogel loaded with iron and nickel oxides under nitrogen gas flowing at 1123K for 30 min. The surface of CX composed of nanosized spherical particles interconnected to form 3D network structure with irregular sizes and shapes of these particles (Fig. 1a) which is similar to that mentioned in our previous studies [5,7]. Fig.1b displays the growth of CNTs on the surface of carbon xerogel as a result in CVD of camphor. As shown in Fig. 1c, the surface of CX-CNTs irregularly covered with Ti particles. The elemental compositions of carbon, oxygen and titanium species in CX-CNTs-Ti nanohybrid by SEM-EDX analysis (weight %) were 80.8, 17.6 and 1.6%, respectively, as displayed in the inset Figure. Thus about 1.6 wt. % of Ti particles is embedded into the matrix of CX-CNTs was obtained.

For more examination, TEM was taken for the CX-CNTs-Ti sample. It was shown that the CNTs with outer diameters ranging from 24 to 46 nm and Ti particles aggregated as black shadow over CX and CNTs were detected.

Fig. 2 illustrates the N_2 adsorption-desorption isotherms of CX-CNTs before and after doping with titanium precursor and the pore parameters are listed in Table 1. According to IUPAC classification [27], N_2 adsorption-desorption

isotherms of both samples are classified as Type IIb representing mesoporous materials. This is because of there is no plateau at high p/p_0 unlike Type IV isotherm. Type IIb is well-characterized by hysteresis loops of type H3 confirming the presence of slit-shaped pores. Obviously the addition of Ti particles led to a considerable decrease in the adsorbed amount of nitrogen, accordingly; the specific surface area is reduced from 81 to 43 m^2/g. Thus the specific surface area of CX-CNTs-Ti is lower than that of CX-CNTs because it possesses less micropores and bigger pore sizes. However, the total pore volume and pore width are considerably increased from 0.126 to 0.250 cm^3/g and from 6.25 to 23.5 nm accompanying with an increase in the mesopore volume also (cf. Table 1), respectively. The mesopore fraction (V_{meso}/V_p, %) was found to be 90.5% for CX-CNTs and 99.2% for CX-CNTs-Ti confirming that the resultant nanohybrids are mesoporous materials. Probably these results caused that

Adsorption of MB onto carbonaceous nanohybrids

Adsorption experiments were carried out by conducting 10 mg of sample with 25 mL of 10 mg/L of MB dye under stirring for 180 min in order to determine the equilibrium time. Fig. 3 shows the adsorption performance of the prepared nanohybrids. With increasing the contact time, the removal of MB dye onto two nanohybrids is steeply increased at the initial few minutes then followed by a slowly increase. CX-CNTs-Ti adsorbent exhibits higher removal efficiency for MB dye of about 86.8% in comparison to that adsorbed by CX-CNTs (~ 70%) at 180 min. Also, the adsorption-desorption equilibrium time of MB onto CX-CNTs and CX-CNTs-Ti in the dark is established at 60 and 30 min, respectively. This finding affirms the high adsorption efficiency of CX-CNTs-Ti. Therefore, an enhancement in the total pore volume and appropriate wider pores due to doping CX-CNTs with Ti particles led to creation of efficient adsorption sites for uptaking MB dye from the aqueous solutions.

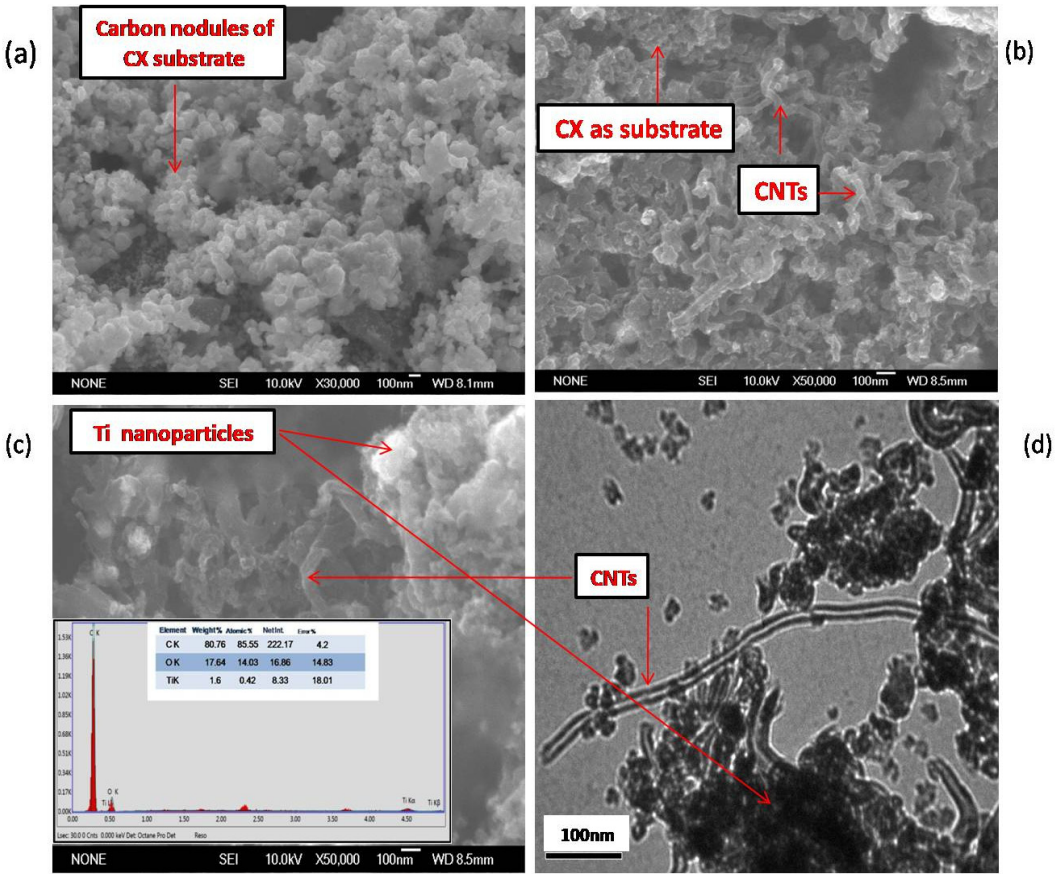

Fig. 1. FE-SEM images for (a) CX and (b) CX-CNTs, and (c) CX-CNTs-Ti nanohybrids (EDX analysis is shown in the insert Figure c).

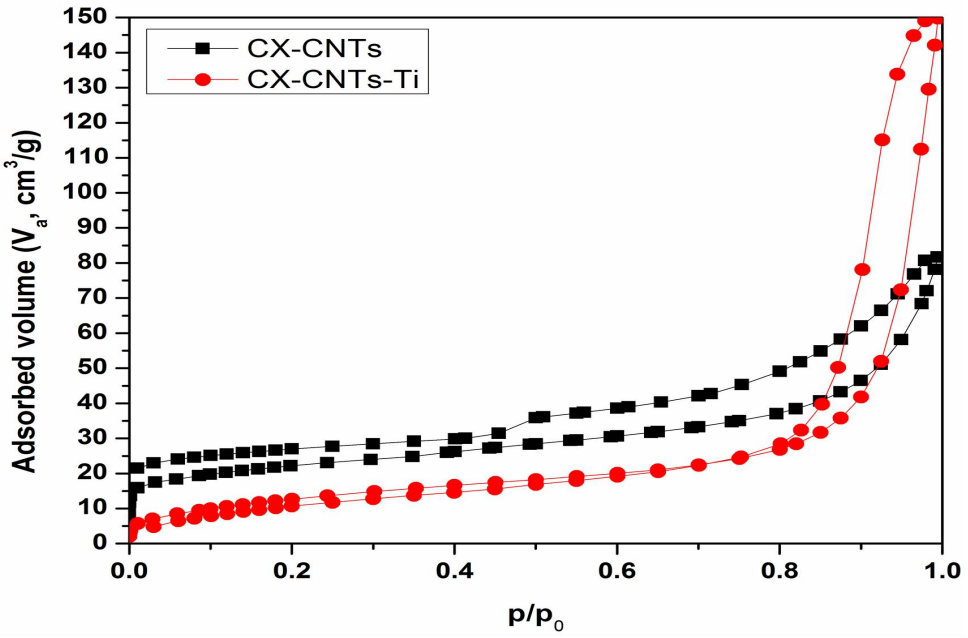

Fig. 2. N_2 adsorption-desorption isotherms of the prepared nanohybrids.

TABLE 1. Pore properties of the prepared nanohybrids.

Sample notation	S_{BET} (m^2/g)	V_P (cm^3/g)	W_P (nm)	$S_{micro\text{-}t\ plot}$ (m^2/g)	$V_{micro\text{-}t\text{-}plot}$ (cm^3/g)	$V_{meso\text{-}t\ plot}$ (cm^3/g)	V_{meso}/V_P %
CX-CNTs	81	0.126	6.25	26.2	0.012	0.114	90.5
CX-CNTs-Ti	43	0.250	23.5	4.2	0.002	0.248	99.2

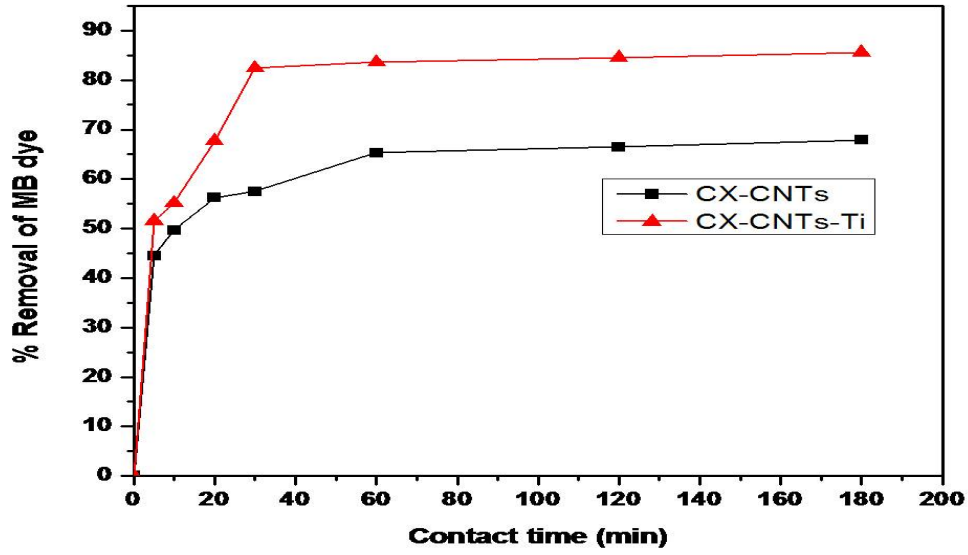

Fig. 3. The removal of MB by CX-CNTs and CX-CNTs-Ti adsorbents under dark condition at pH=6.

Kinetic adsorption studies

Adsorption mechanism of MB dye onto both nanohybrids was achieved by pseudo-first-order, pseudo-second order and intraparticle diffusion models at different initial concentrations of MB dye solution onto varies masses of two nanohybrids. In the pseudo-first-order equation (3), the values of q_{el} and k_1 were calculated from the intercept and slope of *log* $(q_e - q_t)$ *vs. t* plots, respectively as shown in Fig. 4. From pseudo-second-order equation (4), q_{e2} and k_2 values were evaluated by plotting t/q_t *vs. t* as depicted in Fig. 5. In case of intraparticle diffusion equation (5), values of k_{id} and C_i were calculated from the slope and intercept of linear portion of $q_t - t^{1/2}$ plot as shown in Fig. 6.

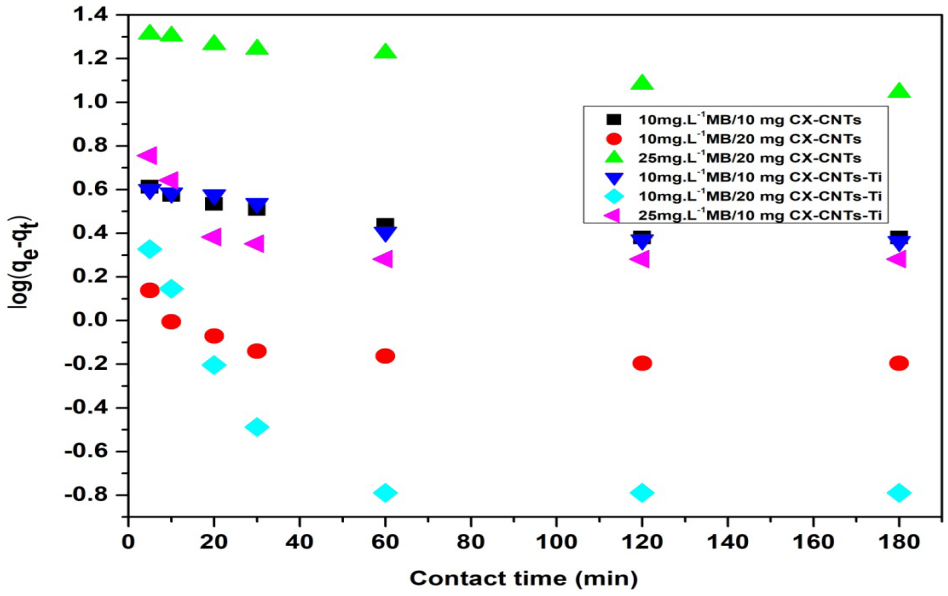

Fig. 4. Pseudo-first order plots of MB adsorbed by two nanohybrids.

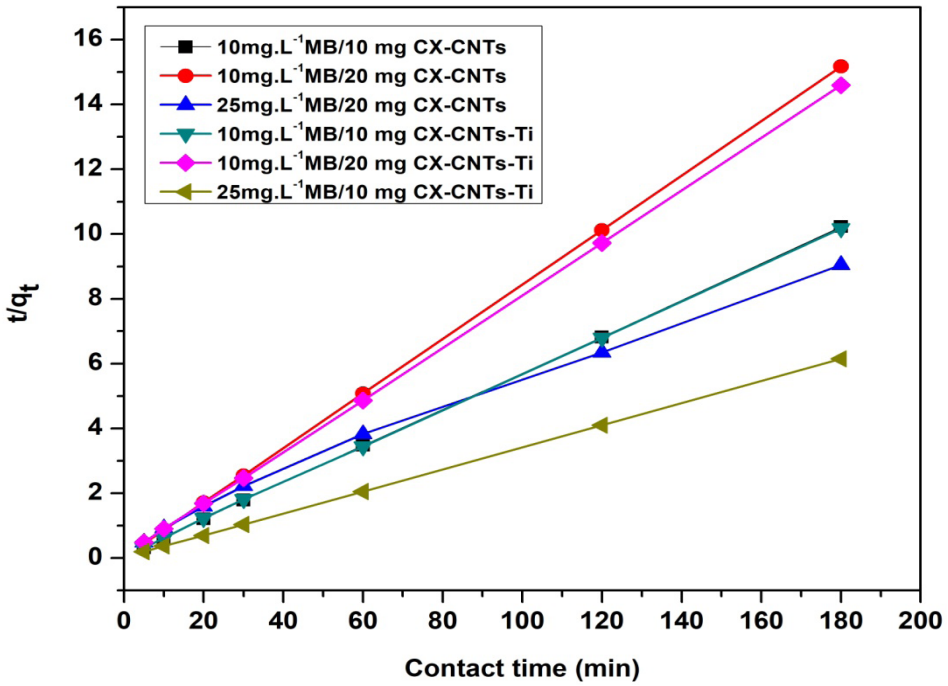

Fig. 5. Pseudo-second order plots of MB adsorbed by two nanohybrids.

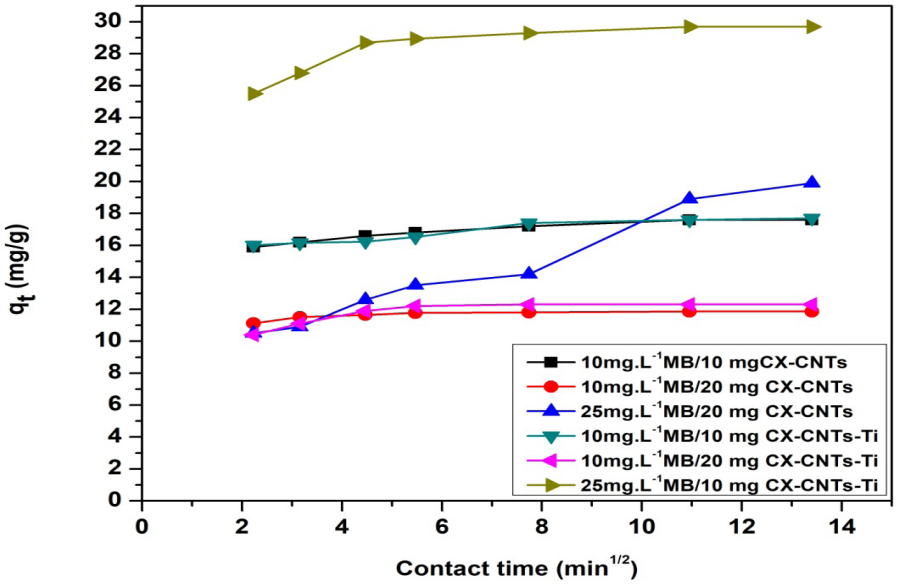

Fig. 6. Intraparticle diffusion plots of MB adsorbed by two nanohybrids.

The applicability of such kinetic models was selected according to the linear regression correlation coefficient, R^2 value, which is listed in Table 2. Inspection of Table 2 as well as Figs. 4 and 5, the fitting of experimental data to the pseudo-first-order model is not so good because it has relative low correlation coefficients (R^2). Accordingly, pseudo-first-order model cannot describe the adsorption results of MB. Conversely, the plots of pseudo-second-order model showed good linear relations with excellent R^2 values close to 1, affirming that the kinetic data significantly fit with of pseudo-second-order model. Thereof, the pseudo-second-order model is more adequate to depict the adsorption of MB dye onto both nanohybrids under dark operation.

Fig. 6 describes the intraparticle diffusion plots at different initial concentrations of MB dye solution onto varies masses of two nanohybrids. The plots clearly show two noticeable intercepting lines. The first is a fast increasing step at beginning, followed by a relatively slow increasing. Thus the adsorption of MB on the nanohybrids is a multi-step process and the intraparticle diffusion is not the only rate-controlling step, but that other processes may control the rate of adsorption.

However, the photocatalytic degradation experiments of MB using both nanohybrids under a visible light irradiation were employed in order to improve the removal percentage and to assess the photocatalytic activity of both nanohybrids.

Photocatalytic activity of carbonaceous nanohybrids

However, most studies have focused on developing of TiO_2 supported on carbon materials for dye photodegradation [28-31]. For the first time, here we studied the photocatalytic performance of Ti particles coated the surface of CX-CNTs nanohybrid.

The photocatalytic activity of both nanohybrids was evaluated by changing the dose of photocatalyst nanohybrids (10 and 20 mg) and the initial concentrations of MB dye (10 and 25 mg/L) at room temperature and at the initial pH 6 of dye. As shown in Fig. 7 (a and b) when the dose increased from 10 to 20 mg with 10 mg/L of MB dye, the removal efficiency increased also form 70 and 88.5% at 180 min to 90 and 99% at 60 min onto CX-CNTs and CX-CNTs-Ti respectively. Upon increasing the initial concentration of MB dye from 10 to 25 mg/L, the removal efficiency reduced from 90 to 43.4% and from 99 to 92.1% at 180 min for MB photocatalytic degradation by those samples, respectively. These findings confirm that the presence of titanium particles is very effective in enhancing the photodegradation of MB dye in aqueous solution under visible light irradiation according to the difference between data plotted in Figs. 3 and 4. Thus the CX-CNTs-Ti sample exhibited higher removal rate at earlier time of MB photodegradation. Therefore, the photocatalyst dose and initial dye concentration have significantly affected the

TABLE 2. Parameters of kinetic models from adsorption of MB dye onto two nanohybrids (T= 298 K, V=25 mL and pH =6).

Samples	Sample mass + C_0 of MB dye	First order kinetic			Second order kinetic			Intraparticle diffusion	
		q_e (mg/g)	k_1 (min^{-1})	R^2	q_e (mg/g)	k_2 (g/mg min)	R^2	K_d (mg/g $min^{0.5}$)	C_i
CX-CNTs	10 mg+10mg/L	17.8	6.91×10^{-4}	0.771	17.8	0.048	1	0.152	15.8
	20mg+10mg/L	2.09	2.30×10^{-3}	0.521	11.9	0.252	1	0.050	11.3
	20mg+25mg/L	15.1	2.30×10^{-3}	0.922	21.3	3.46×10^{-3}	0.987	0.881	8.38
CX-CNTs-Ti	10 mg+10mg/L	3.79	2.30×10^{-3}	0.816	17.8	0.040	0.999	0.168	15.6
	20mg+10mg/L	1.08	0.0115	0.592	12.5	0.097	1	0.136	10.9
	20mg+25mg/L	1.90	0.025	0.384	30.3	0.073	1	0.315	26.2

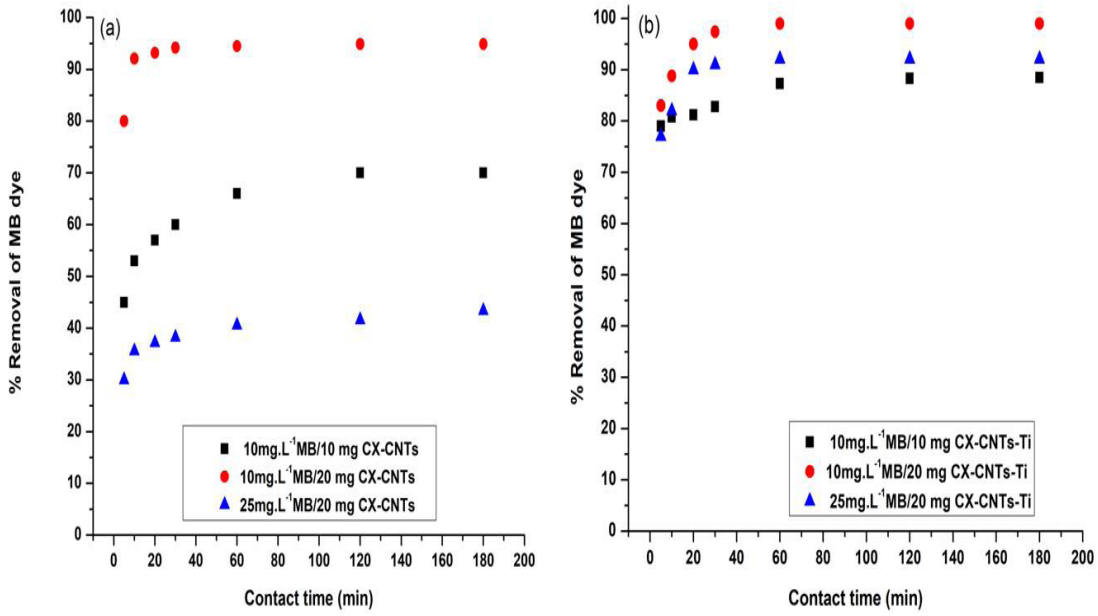

Fig. 7. Removal of MB by two nanohybrids under visible light source at pH=6.

photocatalytic degradation of MB dye as shown in photodegradation curve (Fig. 8). In conclusion, the high performance of both photocatalyst nanocomposites for removing MB dye from aqueous solution in dark and visible light irradiation is due to the synergic effect resulting from the combination of surface functional groups and Ti species as active sites for adsorption and photocatalytic processes.

Conclusions

In this work, nanohybrids of CX-CNTs and CX-CNTs-Ti particles were synthesized successfully as evident by FE-SEM and TEM. It has been found that the specific surface area of CX-CNTs-Ti is lower than that of CX-CNTs because it possesses less micropores and bigger pore sizes. Removal of MB dye by adsorption process is reached to 70% and 86.6% by CX-

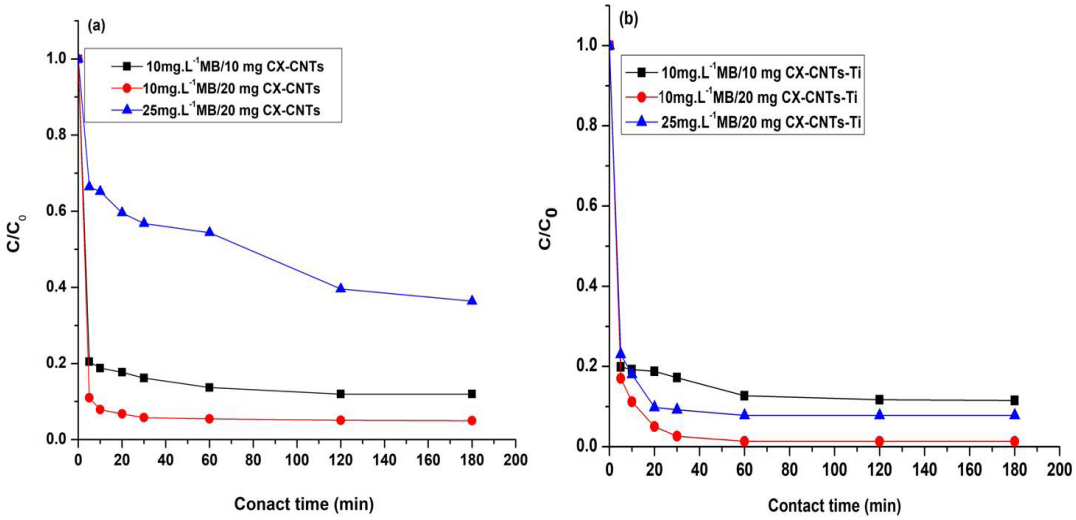

Fig. 8. Photodegradation of MB by two nanohybrids under a visible light source at pH=6.

CNTs and CX-CNTs-Ti samples, respectively. Whereas, the removal of MB dye through photocatalytic condition using CX-CNTs and CX-CNTs-Ti is enhanced to 90 and 99% at 60 min, respectively. Therefore, these results confirm the superior adsorptivity and photoactivity properties of the obtained CX-CNTs-Ti.

Acknowledgement

The authors gratefully acknowledge the financial supports provided by the National Research Centre (NRC), Egypt, under the Project No. **11090201.**

References

1. Pekala R.W., Organic aerogels from the polycondensation of resorcinol with formaldehyde, *J. Mater. Sci.* **24**, 3221-3227 (1989).

2. Celzard A., Fierro V., Amaral-Labat G., *Adsorption by Carbon Gels, in: Novel carbon adsorbents,* edited by Tascón J. M. D., Elsevier Ltd., p. 207 (2012).

3. Halama A., Szubzda B., Pasciak G., Carbon aerogels as electrode materials for electrical double layer supercapacitors – synthesis and properties, *Electrochim. Acta* **55**, 7501–7505 (2010).

4. El-Khatat A.M., Al-Muhtaseb S.A., Advances in Tailoring Resorcinol□Formaldehyde Organic and Carbon Gels, *Adv. Mater.* **23**, 2887-2903 (2011).

5. Girgis B. S., Attia A. A., Abo-El- Enein S. A., Fathy N. A., Synthesis and characterization of porous carbons by the sol-gel method from resorcinol-formaldehyde resin, *Egypt. J. Chem.* **52**, 381-393 (2009).

6. Girgis B.S., El-Sherif I.Y., Attia A.A., Fathy N.A., Textural and adsorption characteristics of carbon xerogel adsorbents for removal of Cu (II) ions from aqueous solution, *J. Non-Cryst. Solids* **358**, 741-747 (2012).

7. Iijima S., Helical microtubules of graphitic carbon, *Nature* **354**, 56-58 (1991).

8. Prasek J., Drbohlavova J., Chomoucka J., Hubalek J., Jasek O., Adam V., Kizek R., Methods for carbon nanotubes synthesis—review, *J. Mater. Chem.* **21**, 15872-15884 (2011).

9. De Volder M. F. L., Tawfick S. H., Baughman R. H., Hart A. J., Carbon nanotubes: Present and future commercial applications, *Sci*. **339**, 535–539 (2013).

10. Eatemadi A., Daraee H., Karimkhanloo H., Kouhi M., Zarghami N., Akbarzadeh A., Abasi M., Hanifehpour Y., Joo S. W., Carbon nanotubes: properties, synthesis, purification, and medical applications, *Nanoscale Res. Lett.* **9**, 1–13 (2014).

11. Attia A.A., Shouman M.A., Sayyah S.M., Fathy N.A., Khaliel A.B., Abas K.M., Sequestration of methylene blue and lead ions by MWCNT modified with polyconducting polymers, *Egypt. J. Chem.* **60**, 221 –241 (2017).

12. El-Khouly S. M., Fathy N. A., Multiwalled-carbon nanotubes supported amorphous Fe2O3- and Ag2O-Fe2O3 as Fenton catalysts for degradation of maxilon red dye, *Asia-Pac. J. Chem. Eng.* **13**, e2184 (2018), https://doi.org/10.1002/apj.2184.

13. Worsley M.A., Pauzauskie P.J., Kucheyev S.O., Zaug J. M., Hamza A. V., Satcher Jr. J. H., Baumann T. F., Properties of single-walled carbon nanotube-based aerogels as a function of nanotube loading, *Acta Mater.* **57**, 5131–5136 (2009).

14. Worsley M.A., Jr Satcher J.H., Baumann T.F., Synthesis and characterization of monolithic carbon aerogel nanocomposites containing double-walled carbon nanotubes, *Langmuir* **24**, 9763–9766 (2008).

15. Fernández P.S., Castro E.B., Real S.G., Visintin A., Arenillas A., Calvo E.G., E.G. Juárez-Pérez E.G., Menéndez A.J., Martins M.E., Electrochemical behavior and capacitance properties of carbon xerogel/ multiwalled carbon nanotubes composites, *J. Solid State Electrochem.* **16**, 1067–1076 (2012).

16. Haghgoo M., Yousefi A.A., Mehr M.J.Z., Celzard A., Fierro V., Léonard A., Job N., Characterization of multi-walled carbon nanotube dispersion in resorcinol–formaldehyde aerogels, *Micropor. Mesopor. Mater.* **184**, 97–104 (2014).

17. Shouman M. A., Fathy N. A., Microporous nanohybrids of carbon xerogels and multi-walled carbon nanotubes for removal of rhodamine B dye, *J. Water Proc. Eng.* **23**, 165–173 (2018).

18. Fu R., Dresselhaus M.S., Dresselhaus G., Zheng B., Liu J., Satcher Jr. J., Baumann T. F., The growth of carbon nanostructures on cobalt-doped carbon aerogels, *J. Non-Cryst. Solids* **318**, 223–232 (2003).

19. Steiner S.A., Baumann T.F., Kong J., Satcher J.H., Dresselhaus M.S., Iron-doped carbon aerogels: novel porous substrates for direct growth of carbon Nanotubes, *Langmuir* **23**, 5161-5166 (2007).

20. Fathy N.A., Annamalai K.P., Tao Y., Effects of phosphoric acid activation on the nanopore structures of carbon xerogel/carbon nanotubes hybrids and their capacitance storage, *Adsorption* **33**, 355–360 (2017).

21. Brunauer S., Emmett P.H., Teller E., Adsorption of gases in multi-molecular layers, *J. Am. Chem. Soc.* **60**, 309-319 (1939).

22. Harkins W.D., Jura G., Surfaces of Solids. XIII. A vapor adsorption method for the determination of the area of a solid without the assumption of a molecular area, and the areas occupied by nitrogen and other molecules on the surface of a solid, *J. Amer. Chem. Soc.* **66**, 1366-1373 (1944).

23. Horvath G., Kawazoe K., Method for the calculation of effective pore size distribution in molecular sieve carbon, *J. Chem. Eng. Japan* **16**, 470–475 (1983).

24. Lagergren S., Zur theorie der sogenannten adsorption geloster stoffe. 591. Kungliga Svenska Vetenskapsakademiens, *Handlingar* **24**, 1–39 (1898).

25. Ho Y.S., McKay G., Sorption of dye from aqueous solution by peat, *Chem. Eng. J.* **70**, 115–124 (1998).

26. Morris J., Weber W.J., Kinetics of adsorption on carbon from solution, *J. Saint Eng. Div. Am. Soc. Civil. Eng.* **89**, 31–39 (1963).

27. Rouquerol F., Rouquerol J., Sing K., *Adsorption by Powders and Porous Solids, Principle, Methodology and Applications,* Academic Press, p. 440 (1999).

28. Jamil T. S., Ghaly M. Y., Fathy N. A., Abd el-halim T. A., Osterlund L., Enhancement of TiO2 behavior on photocatalytic oxidation of MO dye using TiO2/AC under visible irradiation and sunlight radiation, *Sep. Purif. Technol.* **98**, 270–279 (2012).

29. Li X., Lin H., Chen X., Niu H., Zhang T., Liu J., Qu F., Fabrication of TiO2/porous carbon nanofibers with superior visible photocatalytic activity, *New J. Chem.* **39**, 7863-7872 (2015).

30. Zhang Y. H., Tang Z. R., Fu X. Z., Xu Y. J., TiO2-graphene nanocomposites for gas-phase photocatalytic degradation of volatile aromatic pollutant: Is TiO2-graphene truly different from other TiO-carbon composite materials? *ACS Nano,* **4**, 7303–7314 (2010).

31. Azzam E.M.S., Fathy N.A., El-Khouly S.M., Sami R.M., Enhancement the photocatalytic degradation of methylene blue dye using fabricated CNTs/TiO2 /AgNPs/Surfactant nanocomposites, *J. Water Proc. Eng.* **28**, 311-321 (2019).

ازالة صبغة الميثيلين الزرقاء باستخدام مركبات هجين نانومتري من كربون زيروجيل وأنابيب الكربون النانومترية المنشطة بالتيتانيوم

نادي عطية فتحي، سحر احمد الخولي، ريهام محمد ابوالعينين
قسم الكيمياء الفيزيقية - المركز القومي للبحوث - الجيزة - مصر.

تم انتاج هجين نانومتري من الكربون زيروجيل وأنابيب الكربون النانومترية (CX-CNTs) من خلال تقنية سلسة تقوم على تزيين الكربون زيروجيل بأنابيب الكربون النانومترية والتى أنجزت بتلقائية أثناء تفحيم كل من ريزورسينول-الفورمالديهايد زيروجيل عند درجة حرارة ١١٢٣ كلفين والكافور كمصدر لأنابيب الكربون النانومترية عند درجة حرارة ٥٢٣ كلفن. بعد ذلك تم تنشيط الهجين CX-CNTs المحضر باستخدام تيترابيوتيل أورثوتيتانات كمصدر للتيتانيوم لتكوين هجين نانومتري من CX-CNTs-Ti. تم دراسة الخصائص المورفولوجية والنسيجية للعينات باستخدام المجهر الإلكترونى الماسح بالانبعاث (FE-SEM)، المجهر الإلكتروني النافذ عالي الدقة (TEM)وامتزاز غاز النيتروجين عند ٧٧ كلفن. كما تم اجراء دراسة للخواص الضوئية والامتزاز للعينات المحضرة تجاه صبغة الميثيلين الزرقاء. واثبتت النتائج من FE-SEM و TEM تشكيل CNTs على سطح CX وتبين أن الهجين المطور يتمتع ببناء تركيبى ميزوبورس. ووجد أن كفاءة الامتزاز لعينات CX-CNTs-Ti, CX-CNTs تصل الي ٧٠ ٪ و ٨٦,٦ ٪ بقرب ١٨٠ دقيقة على التوالي. كما تم استخدام الضوء المرئي لتعزيز كفاءة CX-CNTs-Ti , CX-CNTs الازالة الصبغة حيث وصلت إلى ٩٠ و ٩٩ ٪ عند ٦٠ دقيقة على التوالي .وهكذا فإن الهجين النانومتري CX-CNTs-Ti أظهر قدرة فائقة على الامتصاص والتكسير الضوئي لإزالة صبغة الميثيلين الزرقاء وذلك يرجع الي وجود جزيئات التيتانيوم على مصفوفة الـ CX-CNTs.كما أدى تنشيط الـCX-CNTs بجزيئات التيتانيوم إلى انخفاض في مساحة السطح المحددة مع تعزيز في حجم المسام الكلي وكمية المسام الأوسع. وعليه فإن الهجين النانومتري CX-CNTs-Ti يظهر كممتز وكمحفز ضوئي فعال تجاه إزالة صبغة الميثيلين الزرقاء من محاليلها المائية.